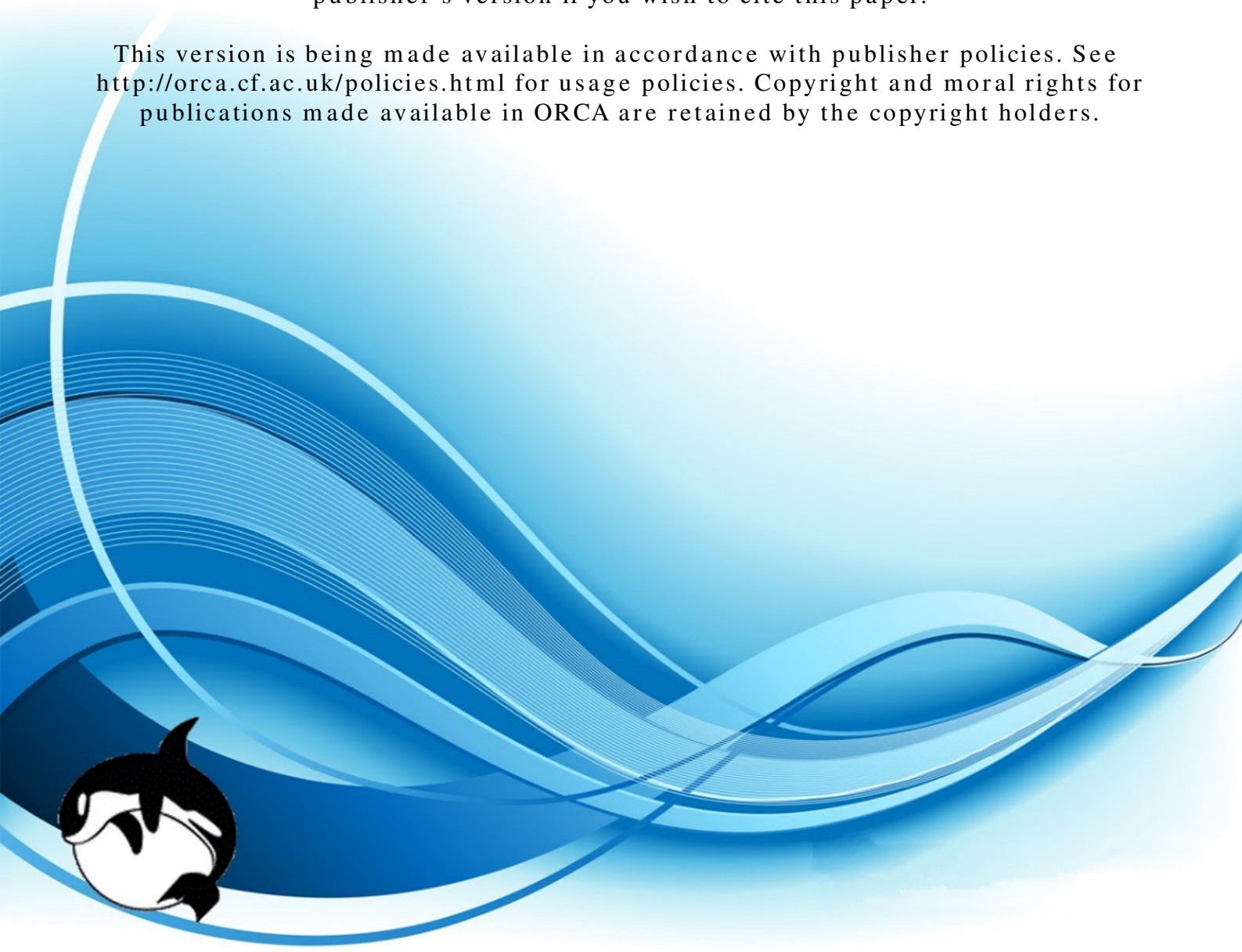

Influence of csgD and ompR on nanomechanics, adhesion forces and curli properties of *E. coli*

by

*Stefano Perni [1], Emily Callard Preedy [1], Paolo Landini [2] and Polina Prokopovich [1 *]*

[1] Cardiff School of Pharmacy and Pharmaceutical Science, Cardiff University, Cardiff, UK

[2] Department of Biomolecular Sciences and Biotechnology, University of Milan, Milan, Italy

Keywords: *E. coli*, Adhesion Forces, Atomic Force Microscope, Bacteria, curli, Freely Jointed Chain Model, OmpR, CsgD

Abstract

Curli are bacterial appendages involved in the adhesion of cells to surfaces; their synthesis is regulated by many genes such as: *csgD* and *ompR*. The expression of the two curli subunits (CsgA and CsgB) in *Escherichia coli* (*E. coli*) is regulated by CsgD, at the same time, *csgD* transcription is under the control of OmpR; therefore, both genes are involved in the control of curli production. In this work, we elucidated the role of these genes on the nanomechanical and adhesive properties of *E. coli* MG1655 (a lab strain not expressing significant amount of curli) and its curli producing mutants overexpressing OmpR and CsgD, employing Atomic Force Microscopy (AFM).

Nanomechanical analysis revealed that the expression of these genes gave origin to cells with lower Young modulus (E) and turgidity (P_0); whilst the adhesion forces were unaffected when genes involved in curli formation were expressed. AFM was also employed to study the primary structure of the curli expressed through the Freely Jointed Chain (FJC) model for polymers. CsgD increased the number of curli on the surface more than OmpR and the over-expression of both genes did not result in a greater number of curli. Neither of the two genes had an impact on the structure (total length of the polymer, number and length of Kuhn segments) of the curli. Our results further suggests that, despite the widely assumed role of curli in cell adhesion, cell adhesion force is dictated also by surface properties as no relation between number of curli expressed on the surface and cell adhesion was found.

Introduction

Microorganisms can colonize surfaces originating three dimensional structures (known as biofilms) where cells properties, such as: growth rate, susceptibility to biocides and proteomic profile, are generally different from their planktonic (floating) count parts [1]; these phenotypical differences are the result of different genes expression patterns [1-3]. Because of their resistance to sanitizing agents and consequent involvement in many infections or contaminations, biofilms are generally perceived negatively [4]. However, properties such higher resistance to toxic chemicals, have been exploited in biotechnological processes as biofilm cells can survive the unfavorable environment, from a biological standpoint, that various chemical reactions require [5,6].

Biofilm formation is a multi-steps process [1,6,7] that has been found to be, not only species specific, but also strain dependent [8]. The initial phase of biofilms formation involves floating cells approaching a surface and establishing a reversible attachment that subsequently turns into an irreversible bond [1]. Flagella, curli fibers and pili are different cell surface features implicated in biofilms formation; depending on the bacterial species, they can either facilitate the initial anchoring of the cell to the surface or enable the cell to actively move towards the surface when in the liquid phase or allow crawling on the surface for already bound cells [9]. In particular for *E. coli,* curli fibers (from now on simply referred to as curli) promote cell-cell adhesion and surface attachment in response to unfavorable environmental signals such as low nutrients, low growth temperature etc.; thus, curli represent a major player in *E. coli* biofilm formation in response to environmental stresses [10].

In *E. coli* the genes responsible for curli formation are organized in two operons (Figure 1): *csgAB* encoding for the two curli components (CsgA and CsgB) and *csgDEFG* involved in their control, assembly and transport [11,12]. Similar operons are also present in Salmonella and they are

denoted *agfAB* and *agfDEFG* [13]. Curlin, the product of *csgA*, along with CsgB, acting as nucleator, are the main components of curli, whilst *csgEFG* encodes for three curling assembly factor [14,15]. It has been found that the expression of these operons is controlled by CsgD [14], a transcription regulator belonging to the FixJ/LuxR family. Moreover, curli expression is triggered at low osmolality as controlled by the OmpR/EnvZ systems [16], is stationary phase dependent as controlled by the σ factor RpoS [17] and is under regulation by CpxA/CpxR that are involved in the response of cellular proteins to acidic pH [18,19].

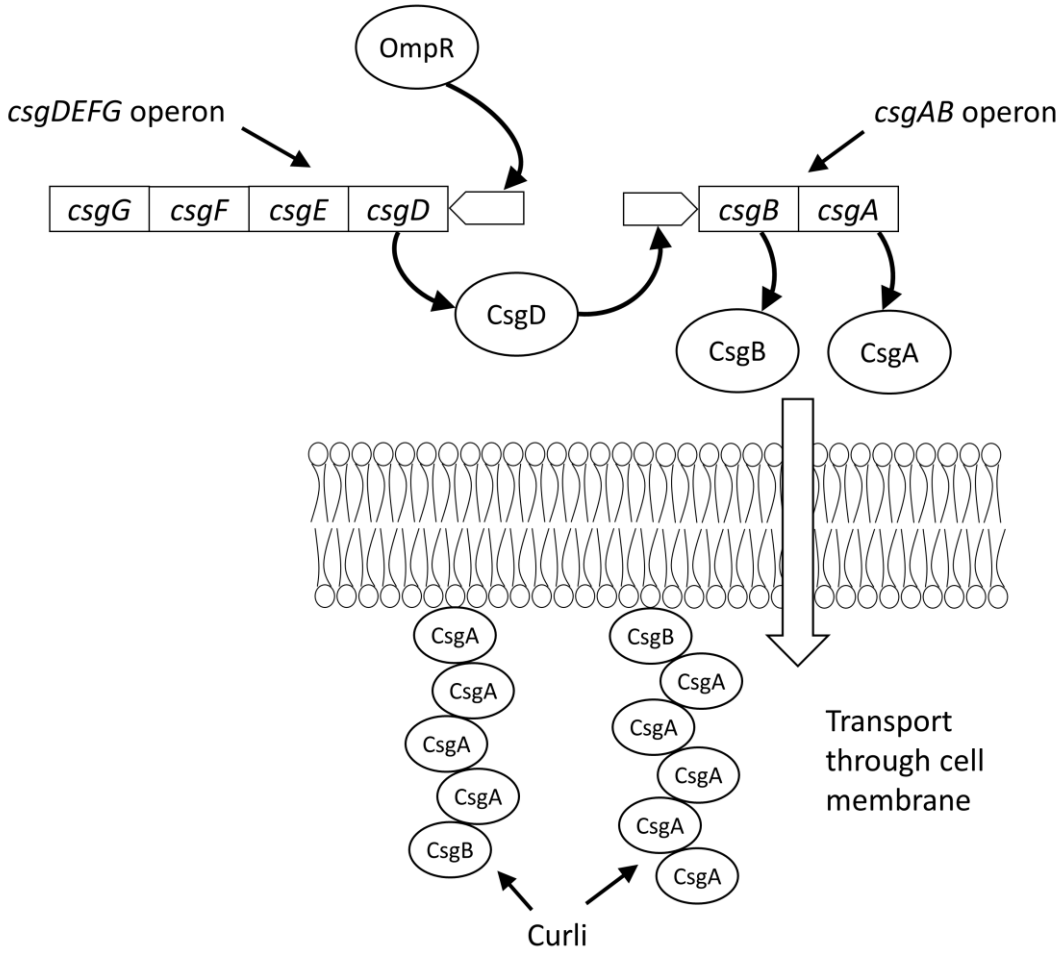

Figure 1.Model of OmpR and CsgD roles in curli synthesis.

OmpR binds the *csgDEFG* operon positively controlling curli expression [20] and the specific mutation of this gene *ompR234* (G to T at position 43 of OmpR, corresponding leucine to arginine substitution) has been shown to increase *E. coli* adhesion to abiotic surfaces through increased curli production [6,20-23]. We have chosen to use in this work *E. coli* MG1655 as it is a widely used curli non-producing strain whereas mutants producing curli through overexpression of *ompR* and *csgD* have been prepared. Because *E. coli* biofilms have relevance in medical and food-borne infections along with biotechnological applications, understanding the role of curli in *E. coli* surface colonization could allow the optimization of this phenomenon to our benefit.

Atomic Force Microscopy (AFM) measures the deformation (and consequently the force exerted) of a cantilever at varying distance from a surface thus allowing the determination of the adhesion forces between two surfaces while a laser beam is deflected off the back of the cantilever [24,25]. AFM has found extensive applications in microbiology [26, 27]; it has allowed to identify virulence properties of pathogens [28,29], and to elucidate the role of specific antigens in adhesion [30] and surface proteins [31]. Moreover, it can be employed in the investigation of both the nanomechanical properties of cells [32-37] and the characterization of the polymeric appendages on the surface as these are described by relations linking the separation distance between the tip and the surface to the force exerted [38-41].

It is generally assumed that curli expression leads to higher cell adhesion to a surface; however, it is still unclear the role of the genes responsible for curli production on their primary structure, number and adhesion forces and whether curli enhance surface adhesion through an increase of the adhesion forces. Our objective was to provide conclusive answers to these questions. In this work, we have studied the effect of two genes responsible for curli production in *E. coli* (*csgD* and *ompR*). Using AFM, we determined the spatial heterogeneity of the

mechanical and adhesive properties of cells not expressing either of these two genes, only one or both of them. Furthermore, the Freely Jointed Chain (FJC) model was fitted to the retraction curves to investigate the role of these two genes on the number and primary structure of the curli produced. This allowed us to investigate the role of *csgD* and *ompR* individually and possible synergistic effects on curli expression. We also tested whether the magnitude of the adhesion forces was related to the number of curli exhibited on the surface.

Materials and Methods

E. coli strains and growing conditions

E. coli MG1655, its *ompR234* mutant (PHL628 [21]) and both strains transformed with pT7-CsgD, a derivative of the pT7-7 plasmid containing the *csgD* gene [22], were used in this study; the essential properties (genotypes and phenotypes) and adopted nomenclature of the strains used in this work are listed in

Table **1**. All *E. coli* strains were stored at 4 °C on Brain Heart Infusion (BHI, Oxoid, UK) plates; for plasmid-bearing strains, ampicillin was added at 100 μg/ml.

10 ml of M63 medium (100 mM KH_2PO_4, 15 mM $(NH_4)_2SO_4$, 0.8 mM $MgSO_4 \cdot 7H_2O$, 9 mM $FeSO_4 \cdot 2H_2O$, 1 mM glucose, adjusted to pH 7.0), supplemented with ampicillin (100 μg/ml) when necessary, were inoculated with a loopful of cells and incubated statically for 24 h at 30°C.

Table 1. Different genotypes and phenotypes of *E. coli* strains used.

Strain	Relevant genotype	Relevant characteristics
MG1655	Reference strain	Reference strain
PHL628	*ompR234* derivative of MG1566	Reference strain Overexpressing OmpR
MG1655 pT7-7CsgD	MG1566 transformed with pT7-7CsgD	Reference strain Overexpressing CsgD
PHL628 pT7-7CsgD	PHL628 transformed with pT7-7CsgD	Reference strain Overexpressing OmpR and CsgD

Cell adhesion quantification

200 µl of the cells suspension prepared as described above were placed in 96 wells plate and incubated for 24 h at 30°C. Each well was rinsed three times with sterile PBS and cells adhering were quantified staining with 0.2 ml of Crystal Violet solution (0.1 % (w/v)) for 15 min. The wells were washed with water three times and 100 µl of ethanol were then added to each well. The crystal violet was allow to dissolve for 1 hour and the optical density of the ethanol solution determined at 570 nm using a UV-vis spectrophotometer.

Gene expression determination by RT-PCR

RNA extraction from bacterial cultures in stationary phase and quantitative real-time PCR experiments were performed as previously described [47]. The relative transcript amounts were determined using 16S rRNA as the reference gene. Results are the average of two technical replicates performed on two biological samples (four experiments in total) and presented normalized against *E. coli* MG1655.

Growth rates determination

10 mL of fresh sterile M63 broth, supplemented with ampicillin (100 μg/ml) when necessary, were inoculated with a loopful of cells and incubated statically at 30°C. After 24 h, 10 μl of each cell suspension were used to inoculate 10 mL of fresh sterile M63 medium, supplemented with ampicillin (100 μg/ml) when necessary. 200 μl from this new suspension were transferred in a well of a 100 wells plate (Bioscreen C, Labsystems, Helsinki, Finland). The bacterial growth curves at 30 °C were recorded every 15 min through optical density (OD) at 600 nm (OD_{600}) using a plate reader (Bioscreen C analyzer; Labsystems, Helsinki, Finland).

All tests were performed in triplicates and on three independent cultures resulting in 9 growth curves for each bacterium. Each growth curve was fitted using the Gompertz growth model to extract values of lag phase and growth rate. Results are presented as mean and standard deviation.

AFM analysis

100 μl of cell suspension were deposited onto a glass (1 x 1 cm) pre-coated with 100 μl of a solution of poly-L-lysine in water 0.1% (w/v) (Sigma) dried overnight. After 30 min the glass was rinsed in PBS three times and was placed in an open liquid cell made of polychlorofluoroethylene, PCTFE (Park Systems, Korea) using PBS as the aqueous environment.

Atomic Force Microscope (AFM) (XE-100 Advanced Scanning Probe Microscope (Park Systems, Korea) was used for adhesion forces measurement using a cantilevers (Veeco, ORC8-

10) with a tip radius of 15 nm and a nominal spring constants ($K_{cantilever}$) of 0.05 N/m; the actual spring constant of the AFM cantilever was determined using the Sader method.

E. coli cells were first located through 5 x 5 μm scans and, after further zoom, 20 approaching and retracting z-piezo coordinates vs. deflection curves without delay were extracted from randomly selected points on the surface of each cell; the force acting on the AFM was calculated from the deflection through the cantilever spring constant. This was repeated for at least 10 cells originated from three individual cultures of each strain resulting in at least 600 (20x10x3) AFM curves for each strain. Results for each parameter are presented as distribution of the >600 values calculated.

Nanomechanics

The approaching part (trace) of the AFM curves was used to calculate the nanomechanical properties of the cells. The Young modulus of the point on the cell surface under investigation was determined fitting the Sneddon variation of the Hertz model to the initial region of indentation between AFM tip and cell surface.

$$F = \frac{2E}{\pi} \frac{\tan\alpha}{\left(1-\nu^2\right)} \delta^2 \qquad (1)$$

where:
F = force recorded by AFM
E = Young modulus
α = the semi-top angle of the tip (18 °)
ν = Poisson ratio
δ = indentation depth

and

$$F = \text{cantilever deflection} * K_{cantilever} \qquad (2)$$

The spring constant of the cell surface (k_b) in the location probed was determined through the slope of the curve after the Hertzian regime.

$$F = k_b \delta \quad (3)$$

where:
F = force recorded by AFM
k_b = spring constant of the cell
δ = indentation depth

Both models require the determination of the separation between cell surface and AFM tip (δ); this was calculated from the coordinates (z-piezo) of the trace curve assuming that the point of contact corresponded to the local minimum of the deflection force; from this:

$$\delta = z - z_0 \quad (4)$$

where:
z_0 = z-piezo value of the minimum of the trace curve
δ = indentation depth

then Eq. 1 and 3 were fitted, using the minimum residual sum of squares method through an in-house written FORTRAN code.

The cell turgidity (pressure difference across membrane) or "turgor pressure" was calculated from the cell spring constant (k_b) as [42,43]:

$$k_b = \beta P_0 \, R \, \varphi(\rho^*) \quad (5)$$

where:
β = $3/2\pi$
P_o = turgor pressure
R = cell radius
ρ^* = reduced tip radius

The reduced tip radius was calculated as [44]:

$$\rho^* = \frac{\rho_0}{\sqrt{\frac{P_o R^3}{2(4\lambda - P_0 R)}}} \quad (6)$$

where:
ρ_0 = AFM tip radius
λ = cell lateral modulus of compression

Furthermore, the function $\varphi(x)$ described in Eq. 5 is [44]:

$$\varphi(x) = x\frac{K_1(x)}{K_0(x)} \quad (7)$$

where K_1 and K_0 are the modified Bessel functions of order 1 and 0, respectively.

Adhesion forces and curli characterization

The adhesion force in each location of the cell surface was determined as the minimum value of the retrace part of the force curve related to that point.

It is assumed that curli are polymeric chains stretched during AFM tip retraction as one extremity is attached to the tip whilst the other is fixed to the cell. The relation between the force required to elongate the polymer and the deformation is measured during AFM retraction, such relation depends on the polymer properties. Increasing applied forces are required with increasing polymer deformations; however, when the applied force reaches the adhesion force between polymer and tip, breaking of the bond between polymer and tip occurs. This phenomenon results in a sudden drop in the force vs. separation distance of the retrace curve (so called polymer rupture). When two or more polymers are initially attached to the AFM tip, the overall stretching process is the combination of the mechanism described for a single chain. In

case the polymers exhibit different properties, the force vs. separation distance curve presents a sequence of polymer stretch/rupture stages resulting in a typical "saw tooth" profile. Each rupture represent one polymeric chain.

Areas of interested (corresponding to a single curli fiber deformation) were first identified as segments of monotonically decreasing interaction force between cell and tip at positive separation distances (no indentation) as described by Polyakov et al. (2011) [40]; then the Freely Jointed Chain (FJC) model was employed to determine the characteristics of the curli expressed in response to the over-expression of CsgD and/or OmpR. The FJC model for a polymer subjected to a pulling force assumes that the polymer chain is made of many rigid segments (Kuhn segments) jointed together; it is described by the following equation:

$$z = -L_C\left(\coth\left(\frac{F\,l_k}{K_{bolt}T}\right) - \frac{K_{bolt}T}{F\,l_k}\right) \tag{8}$$

where:

z	extension of the polymer
L_c	total contour length of the macromolecule
l_k	Kuhn length
K_{bolt}	Boltzmann constant
T	Temperature
F	pulling Force

This is:

$$\frac{z}{L_C} = -\mathbf{L}\left(\frac{F\,l_k}{K_{bolt}T}\right) \tag{9}$$

Where **L** is the Langevin function.

Therefore, Eq. 8 can be expressed in terms of Force vs. Separation distance as:

$$F = -\frac{K_{bolt}T}{l_k}\mathbf{L}^{-1}\left(\frac{z}{L_C}\right) \tag{10}$$

where:
$\mathbf{L}^{-1}$ is the inverse of the Langevin function, this can approximated as:

$$\mathbf{L}^{-1}\left(\frac{z}{L_C}\right) = 3\left(\frac{z}{L_C}\right) + \frac{9}{5}\left(\frac{z}{L_C}\right)^3 + \frac{297}{175}\left(\frac{z}{L_C}\right)^5 + \frac{1539}{875}\left(\frac{z}{L_C}\right)^7 \tag{11}$$

Eq. 10 and 11 can be combined into:

$$F = -\frac{K_{bolt}T}{l_k}\left[3\left(\frac{z}{L_C}\right) + \frac{9}{5}\left(\frac{z}{L_C}\right)^3 + \frac{297}{175}\left(\frac{z}{L_C}\right)^5 + \frac{1539}{875}\left(\frac{z}{L_C}\right)^7\right] \tag{12}$$

Eq. 12 was fitted, using the least squares method, through an in-house written FORTRAN code, to the relevant regions of each retrace curve. Rupture points per each retrace curve were determined as points of local minimum of the retrace curve and this was used to estimate the number of curli expressed by *E. coli* cell on the surface location under AFM analysis.

Once the parameters L_c and l_k for each curli were estimated through the fitting process, the following additional parameters were also calculated:

$N = \frac{L_c}{l_k}$ number of Kuhn segments in the chain (13)

curli density = Number of rupture points (14)

and their distributions determined.

A schematic illustration depicting the procedure employed to analyze the retrace curve is shown in Figure A1.

Statistical analysis

Overall surface heterogeneity of nanomechanical properties, adhesion forces and curli characteristics was investigated through the variance of the measurements on a single cell (20 locations) over the variance of all measurements (20 locations on 30 cells).

Crystal Violet and *csgB* relative expression results were analyzed using ANOVA test followed *post hoc* by Tukey's test individual pairs of data sets ($p<0.05$).

Forces of adhesion were tested for Gaussian distribution using the chi-square test (χ^2 test). In light of the non-normal distribution of the parameters (mechanical, adhesion force and curli); the variations among strains were investigated with the Kruskal-Wallis test followed *post hoc* by Dunn's test for individual pairs of data sets.

Results

Cell growth rate and adhesion quantification

The possible influence of the gene expression alteration on the baseline growth of the strains was investigated as differences in growth rate and lag phase duration could have effect on the quantification of adhering cells. Individual growth curves were fitted with the Gompertz growth model that provided a good match to the experimental data (Figure A2). No variations were observed in the phase duration as results of the overexpression of CsgD (Table 2). The growth rate decreased instead in the curli producing strains (Table 2).

The adhering properties of *E. coli* strains were determined using the crystal violet staining assay (Figure 2a). *E. coli* MG1655, the curli non producing strain, returned the lowest amount of

adhering cells ($p<0.05$); constituting a "base line level" of attachment. The curli producing strain through CsgD over-expression (*E. coli* MG1655 pT7-7CsgD) returned higher adhering cells than the curli producing strain through over-expressing OmpR (*E. coli* PHL628) ($p<0.05$); no difference ($p>0.05$) was found between *E. coli* MG1655 pT7-7CsgD and *E. coli* PHL628 pT7-7CsgD that produces curli through the over-expression of both OmpR and CsgD. CsgD over-expression leads to a 10-fold higher level of *csgBA* mRNA compared to the *ompR234* mutation of PHL628 (Figure 2b).

Table 2. Growth rate and lag phase duration of *E. coli* strains used in M63 medium obtained from fitting Gompertz model to growth curves (n=9).

Strain	Lag phase (hours)	Growth rate ($hours^{-1}$)
MG1655	13.30 ± 0.81	0.0130 ± 0.0005
PHL628	12.40 ± 1.52	0.0061 ± 0.0006
MG1655 pT7-7CsgD	16.33 ± 3.35	0.0044 ± 0.0010
PHL628 pT7-7CsgD	15.13 ± 2.96	0.0036 ± 0.0006

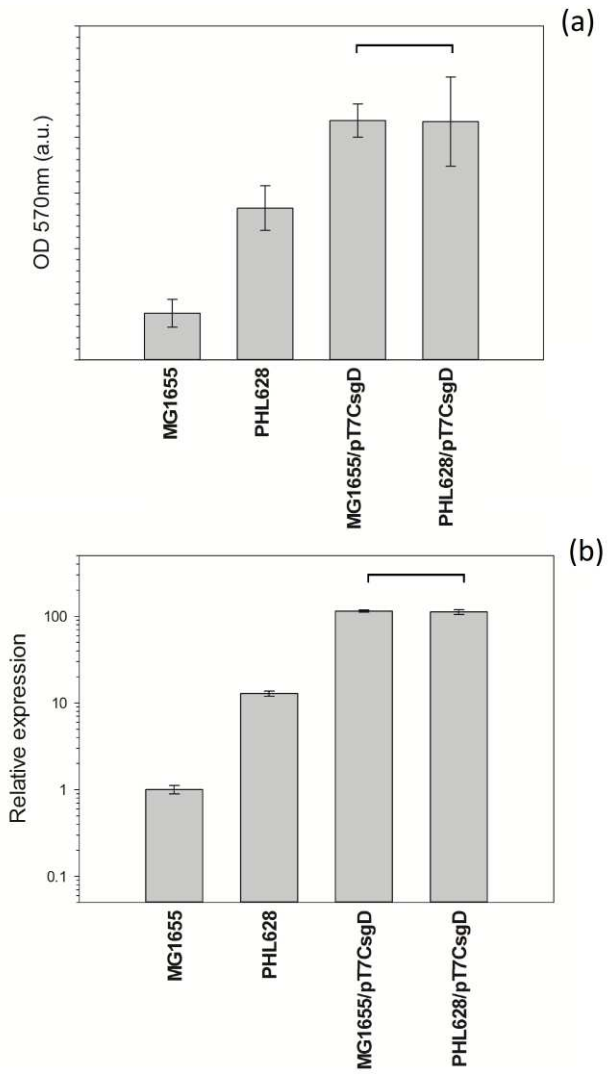

Figure 2. Crystal violet staining of adhering cell of *E. coli* strains (a) and relative expression levels for *csgB* transcript over 16S rDNA (b) in stationary phase cells determined through qPCR. Lines over bar represent groups not significantly different (ANOVA test followed *post hoc* by Tukey's test for individual pairs of data sets). Level of significance p=0.05.

Nanomechanics

The modeling of the AFM approach curve with the Hertz model immediately after the contact between tip and cell gave a good fit and allowed the determination of *E*, whilst the latter part of the curve was well fitted by a linear curve whose slope corresponded to the cell spring constant (used to calculate P_o); an example of such fitting for *E. coli* MG1655 is shown in Figure 3.

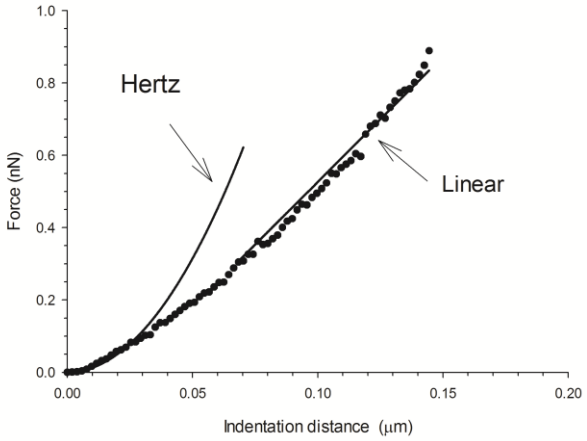

Figure 3. Example of fitting of approach curve with Hertz model and spring constant (linear).

● data ━━ fitting curve

Each parameter determined through AFM in this study was estimated on numerous (20) different locations on the surface of each cell (surface mapping). This allowed us to assess the surface heterogeneity (spatial variation) of every parameter. The variance of the measured values on a single cell was about 80% of the total variance of the measurements carried out on the strain under consideration indicating that the variation was predominantly intracellular than between cells. Figure 4 shows an example of surface mapping of Young modulus (*E*) for *E. coli* MG1655

and spatial heterogeneity is clearly noticeable; further examples for the other strains are presented in Figure A3.

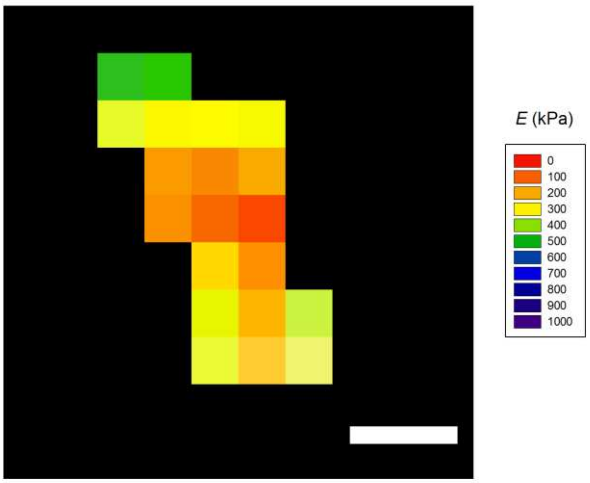

Figure 4. Example of values of Young modulus (*E*) measured on 20 different locations (surface mapping) on the surface of a single cell of *E. coli* MG1655. Bar represent 200 nm.

All strains of *E. coli* employed in this work had values of *E* and P_0 (Figure 5) not following a Gaussian distribution. For *E. coli* MG1655 (reference strain) the median value of the Young modulus was 268 kPa and P_0 equal to 105 kPa, moreover no point on the cell surface had $E > 800$ kPa and $P_0 > 290$ kPa. For *E. coli* PHL628 (over-expressing OmpR) and MG1655 pT7-7CsgD (over-expressing CsgD) the distributions exhibited remarkably lower values for both Young modulus and turgidity. These two strains had median values of *E* about 15 kPa and P_0 about 50 kPa (Figure 5). *E. coli* PHL628 pT7-7CsgD (over-expressing OmpR and CsgD) (Figure 5) had a median values of E of 750 kPa whilst its turgidity had a median value of 560 kPa. *E. coli* MG1655 and PHL628 pT7-CsgD were statistically different from all other strains; PHL628 and MG1655 pT7-CsgD were not different ($p<0.05$).

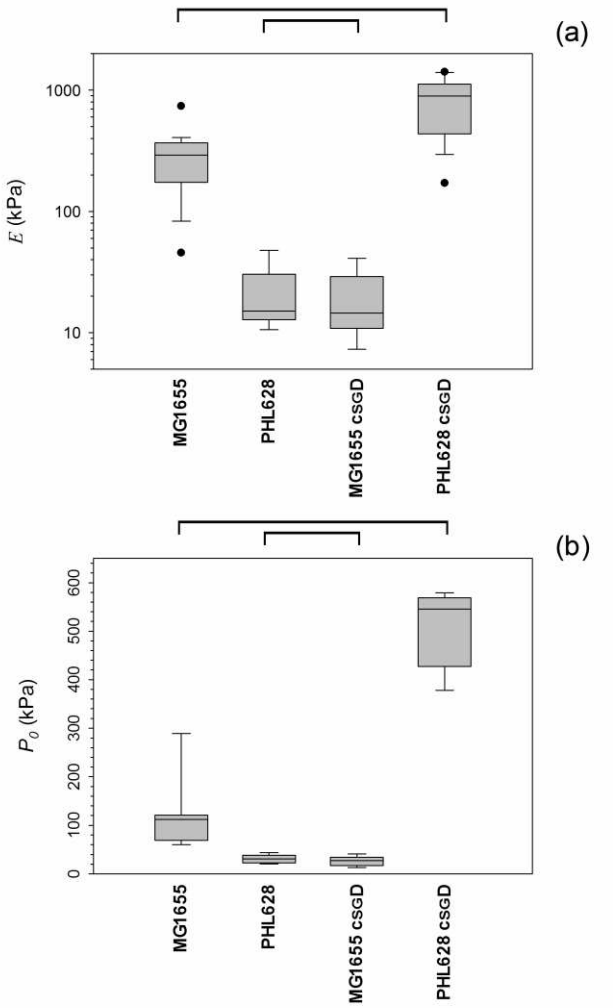

Figure 5. Statistical distribution of the Young modulus (a) and Turgor pressure (b) measured over 20 locations on the surface of several cells of *E. coli*. Lines over bar represent groups not significantly different (Kruskal-Wallis test followed *post hoc* with a Dunn's test for individual pairs of data sets). Level of significance p=0.05.

Adhesion forces

The adhesion force between AFM tip and cell for each location analyzed was determined as the minimum value of force acting on the AFM cantilever during tip retrace. Surface mapping of all strains used in this work, highlighting surface heterogeneity of the adhesion forces, are shown

in Figure A4. The distributions of the adhesion forces for all strains are presented in Figure 6, they appeared not normally distributed in all cases ($p<0.05$). The median adhesion force for *E. coli* MG1655 (reference strain) was 0.4 nN. All strains were not statistically different ($p<0.05$).

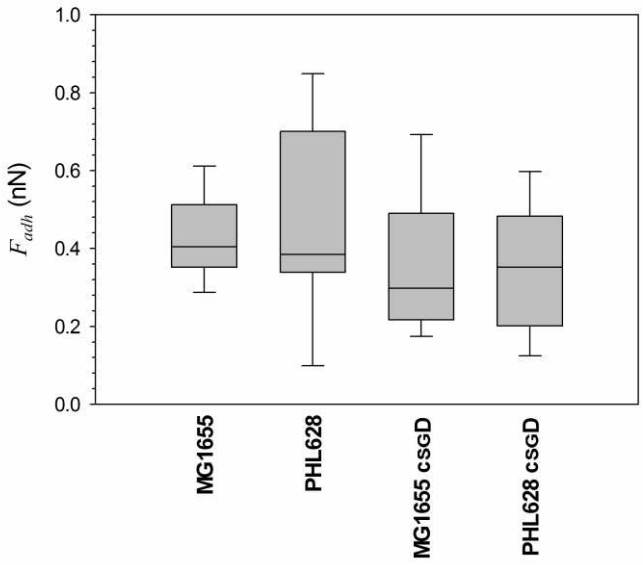

Figure 6. Distributions of adhesion forces measured over 20 locations on the surface of several cells of *E. coli*. Not significant differences found (Kruskal-Wallis test). Level of significance p=0.05.

Curli primary structure analysis

The primary structure of the curli expressed by the *E. coli* cells was investigated through AFM retrace curves. Examples of such retrace curves are shown in Figure 7; it can be seen that the curli non-producing strain *E. coli* MG1655 (Figure 7a) did not show the characteristic "saw tooth" profile related to polymer ruptures. This profile, instead, was evident for *E. coli* strains that produced curli as seen for PHL628 (Figure 7c), MG1655 pT7-7CsgD (Figure 7b) and MG1655 pT7-7CsgD (Figure 7d). Furthermore, it is also noticeable the relative high "goodness of fit" returned by the FJC (Figure 7b, c and d) for each segment of the retrace curve that

corresponded to a curli; this was also quantified through the determination of R^2 between model prediction and experimental data for each curli segment that was generally >0.95. The primary structure of the curli was determined through the estimation of the FJC model parameters. Further examples of retrace curves and FJC model fittings are shown in Figure A5.

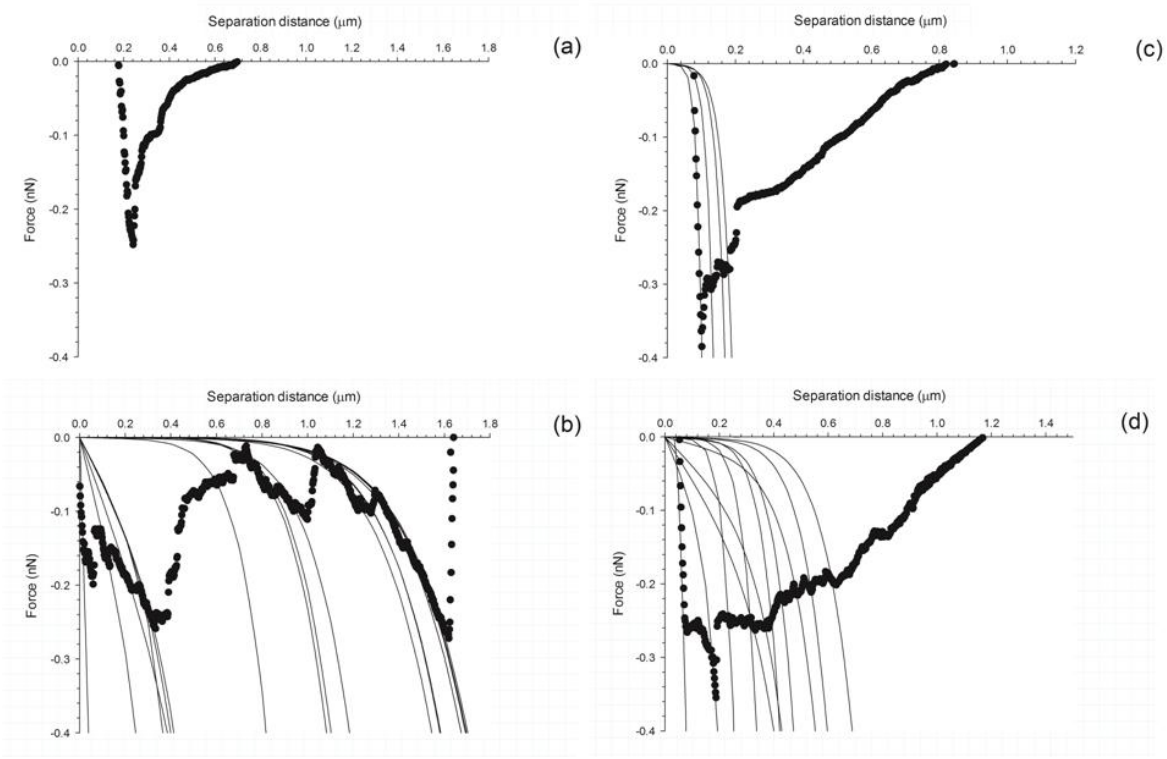

Figure 7. Examples of retrace curves for *E. coli* MG1655 (a), *E. coli* MG1655 pT7-7CsgD (b), *E. coli* PHL628 (c), *E. coli* PHL628 pT7-7CsgD (d) and fitting with FJC.

■ retrace curve ——— FJC fitting

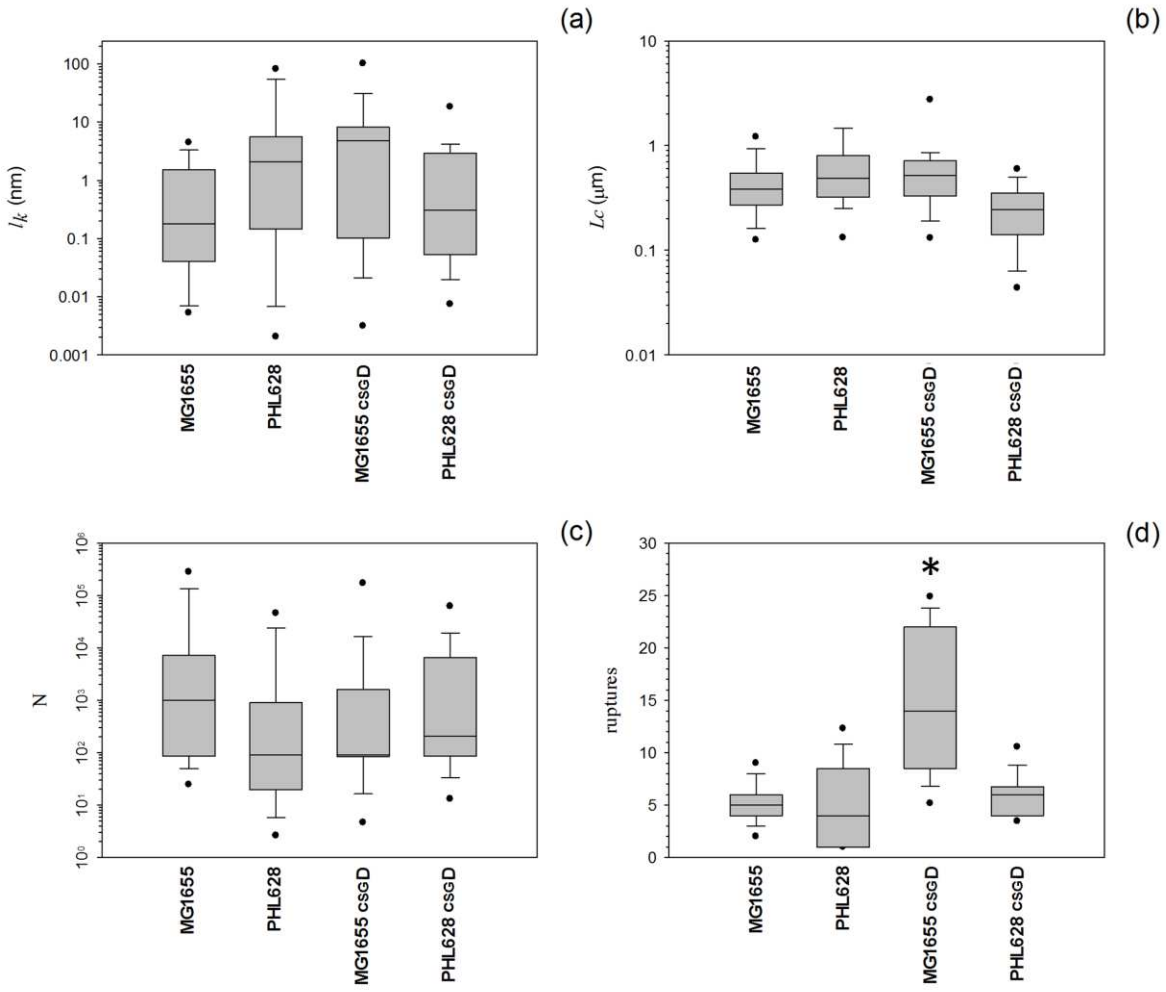

Figure 8. Box and whiskers plots of curli parameters according to FJC. (a) l_k, (b) L_c, (c) N and (d) number of ruptures measured over 20 locations on the surface of several cells of each *E. coli* strains. * represents a group significantly different (Kruskal-Wallis test followed *post hoc* with a Dunn's test for individual pairs of data sets) from the others. Level of significance p=0.05.

The analysis of the AFM retrace curves revealed that the curli produced by all *E. coli* strains used in this work did not exhibit differences ($p>0.05$) in their primary structures as the median values of l_k and L_c were about 0.2 nm and 0.3 μm respectively (Figure 8). Furthermore, the distributions of these parameters did not appear to follow a Gaussian profile. In consequence of these two parameters not varying among the strains used in this work, also the resulting number of Kuhn segments in the curli remained the same at about 1000 units. The most significant difference among the *E. coli* strains used in this work was the median number of ruptures per cell that described the density of curli on the surface. For *E. coli* MG1655 (reference strain) and PHL628 (over-expressing OmpR) this was equal to 4; *E. coli* MG1655 pT7-7CsgD (over-expressing CsgD) exhibited 14 ruptures per curve or more in 50% of the cases and *E. coli* PHL628 pT7-7CsgD (over-expressing OmpR and CsgD) had a median number of ruptures per curve of 6.

Discussion

Cell adhesion results (Figure 2a) are agreement with previously published data [21,22] and with the observation that CsgD over-expression leads to a 10-fold higher level of *csgBA* mRNA compared to the *ompR234* mutation of PHL628 (Figure 2b), thus suggesting a correlation between the two phenomena. Furthermore, also the non curli producing strain (*E. coli* MG1655) was capable of adhering to the substrate, hence the presence of these surface appendages is not essential for adhesion but they are capable of enhancing this phenomenon.

Forces of adhesion measured on chemically homogeneous surfaces are known to display small level of variability, whereas adhesion forces between cells and surfaces exhibit greater level of variability. The origin of these variations can be physical, biological, chemical and practical [29,45];

apart from the practical aspects leading to variability, the other factors are intrinsic and depend on the non-uniform distributions of the composition/concentration of biomolecules on cells surfaces. This hindsight led to the concept of surface mapping of cells properties (not only adhesion forces) also known as heterogeneity of surface properties [29,34-37]. For this reason, on each cell we performed AFM analysis (trace and retrace) on 20 different points on the surface instead of a single one. Moreover, the amount of variation for a single calculated parameter i.e. *E* on a single cell represented about 80 % of the total variation obtained throughout all replicates hence our results re-affirm the non-uniform spatial distribution of bacterial surface parameters (Figure 4, A3 and A4).

AFM is a very powerful tool to study interaction forces in biological systems at the nanoscale level where the biomolecules present on the cells surfaces govern the adhesion properties. Moreover, when polymeric appendages are present on one of the surfaces, the structure of such polymers can be studied through a relation between the force applied to stretch the polymer chain and its structural parameters such as: the length of the chain segments and their overall number [38,40,41]. The heterogeneity of the polymers on a surface results in many segments of the retrace curve, each related to an individual polymer chain, and the characteristic "saw tooth" profile of such curves, where each snap-off (polymer rupture) event corresponds to the breaking of the bond between a specific chain and the counter-surface [28,38-42]. The range of separation distances between tip and cell surface over which curli rupture occurred increased with number of ruptures detected in the retrace curve (Figure 7 and A5). For example, all ruptures for *E. coli* MG1655 (mean values of n = 4) were identifies at separations smaller than 200 nm, whilst for *E. coli* MG1655 pT7-7CsgD7 (mean values of n = 14) ruptures were observed at distance up to 1400 nm. This had an impact on the wider distribution of curli parameter L_c observed (Figure 8).

AFM has also been used to calculate the mechanical properties of cells, modeling the initial part of the indentation curve with the Hertz model; while at greater indentation depths, a linear relation between indentation depth and force has been used [40,41]. This approach derives from the Hertz model assumption of a semi-infinite material; in order to operate when this assumption is valid, an indentation depth of no more than 5-10% of the average cell height was suggested [46]; for deeper indentations a linear response between indentation and applied force was assumed instead. The nature of the AFM tip material has possible implications only on the adhesion forces measurements; whilst the nanomechanical properties and the analysis related to the curli are not influenced by the nature of the tip because the Hertz and FJC models are independent from the material indenting the cell (as long as E of the cell is significant lower than the Young modulus of AFM tip) or stretching the polymeric appendices.

The temperature conditions employed in this work were chosen as curli expression is optimal at 30 °C and almost absent at 37 °C [47]. Furthermore, the growth medium (MG63) and the low glucose concentration were chosen for analogous reasons. The lower growth rate exhibited by the curli producing strains (Table 2) could be linked to the extra metabolic requirements connected to the synthesis of these polymeric chains.

Our results showed that OmpR and CsgD do affect the mechanical properties of the cells outer surface; the much lower E and P_0 of expressing curli (*E. coli* PHL 628 and *E. coli* MG1655 pT7-7CsgD) is probably the result of the increased need to excrete the curli subunits CsgA and CsgB or through the role of CsgD in the regulation of cellulose production [12,47,48]. The values of Young modulus (E) for *E. coli* MG1655 obtained in this work (Figure 5) were similar to those presented by Oh et al. [49] and Chen et al. [50] for other strains of *E. coli*. In general, surface distribution of E is assumed to follow a Gaussian profile [35], whilst not normal distribution for adhesion force and

curli geometrical parameters have been reported [40,41]. Moreover, our result do not agree with the finding of Oh et al. [49] that demonstrated that over and under expression of CsgA in *E. coli* W3110 results in lower *E* than parent cells, again possibly in consequence of CsgD role on cellulose production. Francius et al. [35] measured the mechanical properties of *E. coli* MG1655 expressing *gfp* and reported *E* = 300 kPa that is about the same we found. Nonetheless, as shown in this work that curli alter the surface properties of *E. coli*, also other appendages (adhesins, pili and fimbrie) induce mechanical and electrokinetic changes on cell surfaces [35]. The observation that the PHL628/pT7CsgD strain behaved differently from the other curli-overproducing strains might appear surprising. However, both the *ompR234* mutation and *csgD* overexpression lead to altered expression of genes other than curli, such as genes involved in cellulose production, outer membrane permeability, sugar uptake, etc., in a mutation-specific manner [21,22,36]. Thus, the different effect of the combination of the two mutations in comparison to the behavior of the *E. coli* PHL628 and *E. coli* MG1655/pT7CsgD (Figure 5) would suggest that curli might not be alone responsible for the effects on elasticity and turgor and that OmpR and *csgD* effects on stimulating curli production is not addictive. A possible explanation for this observation could be that elasticity and turgor are properties influenced by the cell wall properties and not just by the presence of appendixes such as curli.

When two bodies are in close proximity the interfacial interactions can result in adhesion; this phenomenon is regulated by chemical-physical parameters and the force required to separate the two bodies is known as "adhesion force" [24,25,51]. Many theories have been developed to study and predict adhesion, i.e. from the fundamental Hertz theory of contact mechanic, the JKR and DMT models have been proposed to take into account the additional contribution of adhesion to interfacial forces between contacting surfaces [24,25]. These theories have been applied successfully

to situations spanning over a range of applications characterized by a very wide characteristic dimension, from the macroscale level of bearings to the nanoscale level of molecules. The forces originated between a cell and a substrate are crucial in determining the colonization of the surface; for examples the greater the force between a bacteria and a material the higher the biofilm formed on such substrate [1].

The geometrical properties determined for the curli were: length (l_k), number (N) of Kuhn segments and the overall length (L_c), whilst the amount of curli expressed was correlated to the number of ruptures observed in the retrace curve. FJC model was chosen to model the relation between curli stretching (Figure 7) and applied force because it was found capable of accurately fit the behavior of bacterial cell appendages [39-41]. Curli overproduction in *E. coli* MG1655 was obtained either by the gain-of-function *ompR234* mutation in the PHL628 strain, in turn leading to increased transcription of the *csgD* gene, or by direct *csgD* overexpression via the pT7CsgD plasmid. Both genes did not appear to modify the structure of these appendages but only their average number (Figure 8). The over-expression of CsgD from pT7CsgD increased the number of curli more than *ompR234* mutation, an observation consistent with the higher levels of *csgD* transcription (data not shown). Furthermore, the effect of these genes on the number of curli was not synergistic as the number of curli in PHL628 pT7-7CsgD was not greater than in MG1566 pT7-7CsgD7. CsgD is a regulator for *csgA* and *csgB* and these genes produce the two subunits of curli (CsgA and CsgB) that are excreted from the cell and assembled into curli [14,15]. Our work shows that neither OmpR nor CsgD are involved in the regulation of the length of the curli. In addition, no correlation was found between the adhesion forces and the number of curli as adhesion forces were unaffected by the production of curli (Figure 6). This result is not in agreement with the established notion that curli enhance surface adhesion through higher

interfacial forces. Interesting, cell adhesion increases with the pattern MG1655 < PHL628 < MG1566 pT7-7CsgD7 = PHL628 pT7-7CsgD (Figure 2); this, along with the similar curli structure and adhesion forces in all strains tested, indicates these parameters are not the only factors related to increased adhesion. For example, surface roughness, concentration of ions in the liquid phase, hydrophobicity/hydrophilicity and shear forces have been shown to be involved in the adhesion of bacteria to surfaces [1].

The effect of OmpR and CsgD on the characteristics of the cell membrane (Figure 5) was also evident in the change of mechanical properties of the cells in response the expression of these genes clearly proving evidence of the involvement of these genes in surface characteristics.

The findings of this work could have application in biotechnology where engineered biofilms are required, therefore, the knowledge of the most adhering strains could provide a higher process yield [6] or in antifouling research elucidating the role and structure of curli.

Conclusions

Biofilm formation is a critical event in many systems, from food safety to infections and biotechnology. Cell adhesion is a complex process regulated by many genes and is governed by the force acting between a substrate and the cell surface. Some of the most noticeable genes involved in *E. coli* adhesion are *ompR* and *csgD* through their regulation of curli production. We have shown that the over-expression of these genes results in heterogeneity of the cell surface. Curli production did not result in higher adhesion forces between cells and AFM tip, furthermore these genes did not result in different curli primary structure but in their number. Mechanical properties (Young modulus and turgidity) of the cell were affected by the expression of these genes. Despite the general assumption that curli are responsible for cell adhesion, changes in

surface chemical-physical properties seem more likely to be the cause of higher cell adhesion than adhesion forces.

The correlation between curli number - adhesion forces - cell adhesion has always been assumed but never tested. We were the first to investigate this and found not to be the case, at least for the *E. coli* strain employed in this work.

Acknowledgments

The authors would like to acknowledge School of Pharmacy and Pharmaceutical Sciences, Cardiff University for a PhD scholarship.

Supporting Information

Schematic description of the curli analysis algorithm, growth curves of all strains, further examples of surface mapping and retraction curves as Supporting Information.

Corresponding author: Dr Polina Prokopovich

School of Pharmacy and Pharmaceutical Science

Cardiff University

Redwood Building, King Edward VII Avenue

Cardiff, UK

CF10 3NB

E-mail address: prokopovichp@cf.ac.uk

References

1. Perni, S.; Callard Preedy, E.; Prokopovich, P. Success and Failure of Colloidal Approached in Bacterial Adhesion. *Adv. Coll. Interface Sci.* **2014**, *206*, 265-274.

2. Orme, R.; Douglas, C.W.; Rimmer, S.; Webb, M. Proteomic analysis of *Escherichia coli* biofilms reveals the overexpression of the outer membrane protein OmpA. *Proteomics* **2006**, *6(15)*, 4269-4277.

3. Resch, A.; Leicht, S.; Saric, M.; Pásztor, L.; Jakob, A.; Götz, F.; Nordheim, A. Comparative proteome analysis of *Staphylococcus aureus* biofilm and planktonic cells and correlation with transcriptome profiling. *Proteomics* **2006**, *6(6)*, 1867-1977.

4. Bos, R., van der Mei, H.C.; Busscher, H.J. Physico-chemistry of initial microbial adhesive interactions--its mechanisms and methods for study. *FEMS Microbiol Rev.* **1999**, *23(2)*, 179-230.

5. Winn, M., Foulkes, J.M.; Perni, S.; Simmons, M.J.H.; Overton, T.W.; Goss, R.J.M. Biofilms and their engineered counterparts: A new generation of immobilised biocatalysts. *Cat. Sci. Tech.* **2012**, *2(8)*, 1544-1547.

6. Perni, S., Hackett, L.; Goss, R.J.M.; Simmons, M.J.; Overton, T.W. Optimisation of Engineered *Escherichia coli* Biofilms for Enzymatic Biosynthesis of L-halotryptophans. *AMB Express* **2013**, *3*, 66.

7. Costerton, J.W., Cheng, K.J.; Geesey, G.G.; Ladd, T.I.; Nickel, J.C.; Dasgupta, M.; Marrie, T. Bacterial biofilms in nature and disease. *Ann. Rev. Microbiol.* **1987**, *41*, 435-464.

8. Perni, S., Aldsworth, T.G.; Jordan, S.J.; Fernandes, I.; Barbosa, M.; Sol, M.; Tenreiro, R. P.; Chambel, L.; Zilhão, I.; Barata, B.; Andrião, A.; Leonor Faleiro, M.; Shama, G.; Andrew. P.W. The Resistance to Detachment of Dairy Strains of *Listeria monocytogenes* from Stainless Steel by Shear Stress is Related to the Fluid Dynamic Characteristics of the Location of Isolation. *Int. J. Food Microbiol.* **2007**, *116(3)*, 384-390.

9. Guttenplan, S.B.; Kearns, D.B. Regulation of flagellar motility during biofilm formation. *FEMS Microbiol Rev.* **2013**, *37(6)*, 849-871.

10. Landini, P. Cross-talk mechanisms in biofilm formation and responses to environmental and physiological stress in *Escherichia coli*. *Res. Microbiol.* **2009**, *160(4)*, 259-266.

11. Barnhart, M.M.; Chapman, M.R. Curli biogenesis and function. *Ann. Rev. Microbiol.* **2006**, *60*, 131-147.

12. Römling, U.; Sierralta, W.D.; Eriksson, K.; Normark, S. Multicellular and aggregative behavior of *Salmonella typhimurium* strains is controlled by mutations in the agfD promoter. *Mol. Microbiol.* **1998**, *28*, 249-264.

13. Römling, U.; Bian, Z.; Hammar, M.; Sierralta, W.D.; Normark, S. Curli fibers are highly conserved between *Salmonella typhimurium* and *Escherichia coli* with respect to operon structure and regulation. *J. Bacteriol.* **1998**, *180*, 722-731.

14. Hammar, M.; Arnqvist, A.; Bian, Z.; Olsen, A.; Normark, S. Expression of two csg operons is required for production of fibronectin- and congo red-binding curli polymers in *Escherichia coli* K-12. *Mol. Microbiol.* **1995**, *18*, 661-670.

15. Hammar, M.; Bian, Z.; Normark, S. Nucleator-dependent intercellular assembly of adhesive curli organelles in *Escherichia coli*. *Proc. Natl. Acad. Sci. USA* **1996**, *93*, 6562-6566.

16. Prigent-Combaret, C.; Vidal, O.; Dorel, C.; Lejeune, P. Abiotic surface sensing and biofilm-dependent regulation of gene expression in *Escherichia coli*. *J. Bacteriol.* **1999**, *181*, 5993-6002.

17. Olsen, A.; Arnqqvist, A.; Hammar, H.; Sukupolvi, S.; Normark, S. The RpoS sigma factor relieves H-NS-mediated transcriptional repression of csgA, the subunit gene of fibronectin-binding curli in *Escherichia coli*. *Mol. Microbiol.* **1993**, *7*, 523-536.

18. Dorel, C.; Vidal, O.; Prigent-Combaret, C.; Vallet, I.; Lejeune, P. Involvement of the Cpx signal transduction pathway of *E. coli* in biofilm formation. *FEMS Microbiol. Lett.* 1**999**, *178*, 169-175.

19. Ogasawara, H.; Yamada, K.; Kori, A.; Yamamoto, K.; Ishihama, A. Regulation of the *Escherichia coli* csgD promoter: interplay between five transcription factors. *Microbiol.* **2010**, *156(8)*, 2470-2483.

20. Prigent-Combaret, C.; Brombacher, E.; Vidal, O.; Ambert, A.; Lejeune, P.; Landini, P.; Dorel, C. Complex regulatory network controls initial adhesion and biofilm formation in *Escherichia coli* via regulation of the csgD gene. *J. Bacteriol.* **2001**, *183(24)*, 7213-7323.

21. Vidal, O.; Longin, R.; Prigent-Combaret, C.; Dorel, C.; Hooreman, M.; Lejeune, P. Isolation of an *Escherichia coli* K-12 mutant strain able to form biofilms on inert surfaces:

involvement of a new ompR allele that increases curli expression. *J. Bacteriol.* **1998**, *180*, 2442-2449.

22. Brombacher, E.; Dorel, C.; Zehnder, A.J.; Landini, P. The curli biosynthesis regulator CsgD co-ordinates the expression of both positive and negative determinants for biofilm formation in *Escherichia coli*. *Microbiology* **2003**, *149(10)*, 2847-2857.

23. Prigent-Combaret, C.; Prensier, G.; Le Thi, T.T.; Vidal, O.; Pejeunne, P.; Dorel, C. Developmental pathway for biofilm formation in curli-producing *Escherichia coli* strains: role of flagella, curli and colonic acid. *Environ. Microbiol.* **2000**, *2*, 450-464.

24. Prokopovich, P.; Perni, S. Comparison of JKR- and DMT- Based Multi-asperity Adhesion Model: Theory and Experiment. *Coll. Surf. A* **2011**, *383(1-3)*, 95-101.

25. Prokopovich, P.; Perni, S. Multi-asperity Contact Adhesion Model for Universal Asperity Height and Radius of Curvature Distributions. *Langmuir* **2010**, *26(22)*, 17028-17036

26. Dorobantu, L.S.; Gray, M.R. Application of atomic force microscopy in bacterial research. *Scanning* **2010**, *32(2)*, 74-96.

27. Lower, S.K. Atomic Force Microscopy to Study Intermolecular Forces and Bonds Associated with Bacteria. *Adv. Exp. Med. Biol.* **2011**, *715*, 285-299.

28. Park, B.J.; Haines, T.; Abu-Lail, N.I. A correlation between the virulence and the adhesion of *Listeria monocytogenes* to silicon nitride: an atomic force microscopy study. *Coll. Surf. B* **2009**, *73(2)*, 237-243.

29. Park, B.J.; Abu-Lail, N.I. Atomic force microscopy investigations of heterogeneities in the adhesion energies measured between pathogenic and non-pathogenic Listeria species and

silicon nitride as they correlate to virulence and adherence. *Biofouling* **2011**, *27(5)*, 543-559.

30. Strauss, J.; Burnham, N.A.; Camesano, T.A. Atomic force microscopy study of the role of LPS O-antigen on adhesion of *E. coli*. *J. Mol. Recognit.* **200**9, *22(5)*, 347-355.

31. Ivanov, I.E.; Boyd, C.D.; Newell, P.D.; Schwartz, M.E.; Turnbull, L.; Johnson, M.S.; Whitchurch, C.B.; O'Toole, G.A.; Camesano, T.A. Atomic force and super-resolution microscopy support a role for LapA as a cell-surface biofilm adhesin of *Pseudomonas fluorescens*. *Res. Microbiol.* **2012**, *163(9-10)*, 685-691.

32. Gaboriaud, F.; Bailet, S.; Dague, E.; Jorand, F. Surface Structure and Nanomechanical Properties of *Shewanella putrefaciens* Bacteria at Two pH values (4 and 10) Determined by Atomic Force Microscopy. *J. Bacteriol.* **2005**, *187(11)*, 3864-3868.

33. Gaboriaud, F.; Dufrêne, Y.F. Atomic force microscopy of microbial cells: application to nanomechanical properties, surface forces and molecular recognition forces. *Coll. Surf. B* **2007**, *54(1)*, 10-19.

34. Cerf, A.; Cau, J.; Vieu, C.; Dague, E. Nanomechanical Properties of Dead or Alive Single-Patterned Bacteria. *Langmuir* **2009**, *25(10),* 5731-5736.

35. Francius, G.; Polyakov, P.; Merlin, J.; Abe, Y.; Ghigo, Y.M.; Merlin, C.; Beloin, C.F. Bacterial Surface Appendages Strongly Impact Nanomechanical and Electrokinetic Properties of *Escherichia coli* Cells Subjected to Osmotic Stress. *PLoS One* **2001**, *6(5)*, e20066.

36. Gualdi, L.; Tagliabue, L.; Landini, P. Biofilm formation-gene expression relay system in *Escherichia coli*: modulation of sigmaS-dependent gene expression by the CsgD regulatory protein via sigmaS protein stabilization. *J. Bacteriol.* **2007**, *189(22)*, 8034-8043.

37. Hu, Y.; Ulstrup, J.; Zhang, J.; Molin, S.; Dupres, V. Adhesive properties of *Staphylococcus epidermidis* probed by atomic force microscopy. *Phys. Chem. Chem. Phys.* **2011**, *13(21)*, 9995-10003.

38. Abu-Lail, N.I.; Camesano, T.A. Polysaccharide properties probed with atomic force microscopy. *J. Microsc.* **2003**, *212*, 217-238.

39. Camesano, T.A.; Abu-Lail, N.I. Heterogeneity in bacterial surface polysaccharides, probed on a single-molecule basis. *Biomacromol.* **2002**, *3(4)*, 661-667.

40. Polyakov, P.; Soussen, C.; Duan, J.; Duval, J.F.; Brie, D.; Francius, G. Automated force volume image processing for biological samples. *PLoS One* **2011**, *6(4)*, e18887.

41. Quilès, F.; Polyakov, P.; Humbert, F.; Francius, G. Production of extracellular glycogen by *Pseudomonas fluorescens*: spectroscopic evidence and conformational analysis by biomolecular recognition. *Biomacromol.* **2012**, *13(7)*, 2118-2127.

42. Arnoldi, M.; Fritz, M.; Bauerlein, E.; Radmacher, M.; Sackmann, E.; Boulbitch, A. Bacterial turgor pressure can be measured by atomic force microscopy. *Phys. Rev. E. Stat. Phys. Plasmas Fluids Relat. Interdiscip. Topics* **2000**, *62(1 Pt B)*, 1034-1044.

43. Boulbitch, A. Deformation of the envelope of a spherical gram-negative bacterium during the atomic force microscopic measurements. *J. Electron. Microsc. (Tokyo)* **2000**, *49(3)*, 459-462.

44. Yao, X.; Walter, J.; Burke, S.; Stewart, S.; Jericho, M.H.; Pink, D.; Hunter, R.; Beveridge, T.J. Atomic force microscopy and theoretical considerations of surface properties and turgor pressures of bacteria. *Coll. Surf. B: Biointerfaces* **2002**, *23*, 213-230.

45. Dorobantu, L.S.; Bhattacharjee, S.; Foght, M.J.; Gray, M.R. Atomic force microscopy measurement of heterogeneity in bacterial surface hydrophobicity. *Langmuir* **2008**, *24(9)*, 4944-4951.

46. Titushkin, I.; Cho, M. Modulation of cellular mechanics during osteogenic differentiation of human mesenchymal stem cells. *Biophys J.* **2007**, *93(10)*, 3693-702

47. Gualdi, L.; Tagliabue, L.; Bertagnoli, S.; Ieranò, T.; De Castro, C.; Landini, P. Cellulose modulates biofilm formation by counteracting curli-mediated colonization of solid surfaces in *Escherichia coli*. *Microbiol.* **2008**, *154(7)*, 2017-2024.

48. Jonas, K.; Tomenius, H.; Kader, A.; Normark, S.; Römling, U.; Belova, L.M.; Melefors, O. Roles of curli, cellulose and BapA in Salmonella biofilm morphology studied by atomic force microscopy. *BMC Microbiol.* **2007**, *7*, 70.

49. Oh, Y.J.; Cui, Y.; Kim, H.; Li, Y.; Hinterdorfer, P.; Park, S. Characterization of curli A production on living bacterial surfaces by scanning probe microscopy. *Biophys. J.* **2012**, *103(8)*, 1666-1671.

50. Chen, Y.Y.; Wu., C.C.; Hsu, J.L.; Peng, H.L.; Chang, H.Y.; Yew, T.R. Surface rigidity change of *Escherichia coli* after filamentous bacteriophage infection. *Langmuir* ***2009,*** *25*, 4607-4614.

51. Prokopovich, P.; Starov, V. Adhesion models: from single to multiple asperity contacts. *Adv. Coll. Interface Sci.* **2011**, *168(1-2)*, 210-222.